Evolution of Nanoscale Zero-valent Iron (nZVI) in Water: Microscopic and Spectroscopic Evidence on the Formation of Nano- and Micro-structured Iron Oxides

Airong Liu *, Jing Liu, Jinhao Han, Wei-xian Zhang*

State Key Laboratory for Pollution Control and Resource Reuse

College of Environmental Science and Engineering

Tongji University，Shanghai, China, 200092

Abstract

Knowledge on the transformation of nanoscale zero-valent iron (nZVI) in water is essential to predict its surface chemistry including surface charge, colloidal stability and aggregation, reduction and sorption of organic contaminants, heavy metal ions and other pollutants in the environment. In this work, transmission electronic microscopy (TEM), X-ray diffraction (XRD) and Raman spectroscopy are applied to study the compositional and structural evolution of nZVI under oxic and anoxic conditions. Under anoxic conditions, the core-shell structure of nZVI is well maintained even after 72 h, and the corrosion products usually contain a mixture of wustite (FeO), goethite (*α*-FeOOH) and akaganeite (*β*-FeOOH). Under oxic conditions，the core-shell structure quickly collapses to flakes or acicular-shaped structures with crystalline lepidocrocite (γ-FeOOH) as the primary end product. This work

* To whom correspondence should be addressed. Tel: +86-21-6598-2684; Fax: +86-21-6598-3689 E-mail address: liuairong@tongji.edu.cn (Airong Liu)

* zhangwx@tongji.edu.cn (Wei-xian Zhang)

provides detailed information and fills an important knowledge gap on the physicochemical characteristics and structural evolution of engineered nanomaterials in the environment.

Keywords: Nanoscale zero-valent iron; Evolution; Oxic water; Anoxic water

1. Introduction

Nanoscale zero-valent iron (nZVI) is an engineered nanomaterials widely used in environmental remediation and hazardous waste treatment [1-4]. nZVI has a classic core-shell structure, which consists of a metallic iron core encapsulated by a thin iron oxide shell of a few nanometers [5]. This core-shell nanomaterial with two nano-constituents has multifaceted functions for contaminant separation and transformation. The metallic iron core serves as an electron source and exerts a reducing character, whereas the oxide shell promotes the adsorption of contaminants via electrostatic interactions and surface complexation [6].

In wastewater treatment and groundwater remediation, nZVI can partially or completely transform from metal iron (Fe^0) to nontoxic iron oxide/hydroxides commonly found in sediments and soils, resulting in significant variations in the nanoparticle structure and composition. The iron oxidation or corrosion also varies depending on the type of irons, contaminants, solution composition and environmental conditions [11-20]. For example, an nZVI (e.g., RNIP from Toda Kogyo Corp.) produced by the hydrogen reduction of ferric oxides [13], the iron oxide shell generated by the gradual exposure to the atmosphere could inhibit

further oxidation of the nZVI particles [14]. The shell-modified RNIP particles formed new iron minerals, goethite, Fe (0) and magnetite when put into water [15]. Research on the chemical transformation of nZVI in groundwater treatment suggested that the differences in groundwater chemistry such as pH, carbonate and phosphate can affect the corrosion products [16-20]. For example, in our previous study, the aging effect of nZVI nanoparticles synthesized by borohydride reduction of $FeCl_3$, was investigated over a period of 90 days in static water [21]. Similarly, nZVI was oxidized primarily to the iron oxide-hydroxide lepidocrocite under flowing aerated water [22]. Results showed that the structure, shape and composition of nZVI changed with time after exposed to water. New applications of nZVI for industrial wastewater treatment provide new challenges on the study of its aging effects [23, 24]. In the reactors for industrial water treatment, the nZVI suspension is typically agitated intensely to achieve uniform dispersion in water. The corrosion products under this condition not only affect its removal capacity, but also the final state and fate of iron materials after their emplacement. Until now, comprehensive study of corrosion products for nZVI under oxic and anoxic water is limited, and is clearly needed to enhance our understanding on the longevity, reactivity, fate, transport and potential toxicity of nZVI.

Objectives of this study are to investigate the chemical transformation, morphological and structural evolution of nZVI under both oxic and anoxic conditions. Fresh- and aged- nZVIs are characterized with transmission electron microscopy (TEM), X-ray diffraction (XRD) and Raman spectroscopy.

Results obtained can contribute to the expanded understanding of nZVI geochemical recycling, oxidation mechanisms, kinetics, and more importantly, the final products and fate of nZVI in the environment.

2. Experimental

2.1 Materials and chemicals

All chemicals used in the study, for example, $FeCl_3 \cdot 6H_2O$ (≥99%) and $NaBH_4$ (≥98%), were analytical grade or better, and all were obtained from Sigma-Aldrich. Chemical stock solutions were prepared using deionized water. Ultrahigh-purity N_2 (≥99.999%) was used to strip dissolved oxygen in water.

2.2 Preparation of fresh and aged nZVI

Procedures used in the preparation of iron nanoparticles have been published previously [5, 6]. In brief, it entailed slowly adding a 1:1 volume ratio of 0.25 M sodium borohydride into 0.045 M ferric chloride solution. The jet-black nanoparticles were collected by vacuum filtration and refrigerated in a sealed polyethylene container in 95% ethanol until use. The residual water content of the nanoparticles as used typically varied between 40 and 50%. Average size of the synthesized nZVI was 60 nm [6]. The nZVI produced had surface areas in the range of 20–40 m^2/g. Iso-electric point (IEP) of nZVI in water was found to be near pH of 8.3 [25].

Corrosion products of nZVI under oxic water were produced by charging fresh nZVI (0.5 g) into deionized water (100 mL), vigorously stirred with an agitator at 300 rpm under ambient conditions. At certain time intervals, the reacted nZVIs were separated, and then stored in ethanol until use.

Corrosion products of nZVI under anoxic water were prepared by putting

fresh nZVI (0.5 g) into sealed serum bottles containing 100 mL of deionized water (previously degassed using N_2). The aging time was 2 h, 6 h, 12 h, 24 h, and 72 h at room temperature (± 0.5℃). The products were then separated and stored in ethanol until use.

2.3 Solid-phase characterization of fresh nZVI and aged nZVI

High-resolution TEM analyses were performed using a TEM 2100 FXII (JEOL, Japan) operated at 200 kV and with selected area electron diffraction (SAED). Specimens were prepared for TEM analysis by allowing a drop of nZVI suspension in ethanol to evaporate onto a carbon film. The samples were then put into a vacuumed box until the ethanol was evaporated.

XRD analyses were conducted using a D8 Advance X (Bruker, Germany), operated at 40 KV and 40 mA with Cu Kα. Samples were prepared by pressing the nZVI particles onto the glass plates for XRD analysis. Continuous scans from 10 to 80° at 2θ were collected with a step size of 0.01° and a count time of 0.2 s per step.

Raman spectra were obtained using a LabRam-1B (Jobin Yvon, France) with a 632 nm He-Ne laser. The samples were put onto glass plates for Raman analysis. Approximately 1 mW of laser irradiation was used to excite the samples. Spectra were collected over the range 4000 – 100 cm^{-1} and averaged over 10 scans, each with an exposure time of 10 s.

2.4 pH and E_h measurements

100 mL of distilled water was added to a four-neck flask fitted with a

customized rubber stopper containing ports for pH and oxidation-reduction potential (ORP) electrodes and sampling. A variable speed mixer set at 300 rpm helped to ensure well-mixed conditions. Measured dissolved oxygen levels were generally less than 0.1 $mg \cdot L^{-1}$ after 30 min of N_2 purging. Then the nZVI was put into the flask to form the suspension with the concentration of 100 $mg \cdot L^{-1}$. A pH (PHSJ-4F) and ORP meter (ORP501, Shanghai REX Instrument Factory) were put into the suspension to monitor the pH and standard potential. Measured redox potential readings (mV) were converted to E_h, the potential relative to the standard hydrogen electrode, as a function of solution temperature by adding +202 mV at 25 ℃ to the ORP values.

3. Results and Discussion

3.1. TEM imaging analysis

Fig. 1 presents high-resolution TEM images that illustrate the changes of particle morphology of nZVI under oxic and anoxic conditions. As shown in Fig.1a, fresh nZVI particles synthesized by the borohydride reduction method aggregate to form chain-like structures with length on the order of a few micrometers due to magnetic and electrostatic interactions. The core-shell structure of the single particle can be observed clearly (Figs. 1b and 1c), that is, a metallic iron core surrounded with a thin iron oxide shell (2~4 nm). As shown in Fig. 1c, when nZVI is placed in anoxic water for 72 h, the core-shell structure is well maintained similar with that of fresh nZVI. Under anoxic condition, the rate of oxidation for nZVI is slow. These findings support that nZVI likely has a long life-time in the subsurface environment.

The nZVI particles are still spherical with the majority in the size range of

50–100 nm after reactions for 2 h under oxic condition (Fig. 1d). With the progress of aging time from 6 to 24 h (Fig. 1e-g), the fraction of the core-shell structures decreases while amorphous spheres are observed. When the nZVI particles were put into the static water for a certain number of days, a complete loss of the Fe(0) core and the appearance of hollowed-out oxide shells were observed [22]. The small dot-like structures in Fig. 1e–i illustrate the possible dissolution-precipitation mechanism responsible for the corrosion product formation. Iron oxides in the amorphous spheres can first dissolve to Fe(II)/Fe(III), and then reprecipitate into an iron hydroxide phase. This in turn evolves to the apparent crystallite phase over a longer time period. The amorphous iron oxides are energetically unstable and eventually replaced by a thermodynamically more stable crystallite phase according to the Gay-Lussac-Oswald ripening rule on oxidation and corrosion of metallic iron to Fe(III) oxide/hydroxide [26].

Some flaky substances can be observed in Fig. 1f and the quantities increase with the progress of the aging time. Although some particles are still circular even for the nZVI aged for 24h (Fig. 1g), the core-shell structure almost disappears (Fig. 1h). According to the XRD patterns as in Fig. 2, the circular spheres for 24-h particles are composed of iron oxides, magenetite/maghemite. The sizes of flaky-shaped substances dominated with the several micrometers, become much larger with the progress of aging time. Fig. 1h and 1i depict the images of nZVI particles aged in oxic water for 48 h and 72 h, respectively, with lepidocrocite accounting for the presence of flaky structures [10,27]. The SAED patterns of the corrosion products after 72-h-aging indicate that the flaky structures are single-crystal phase.

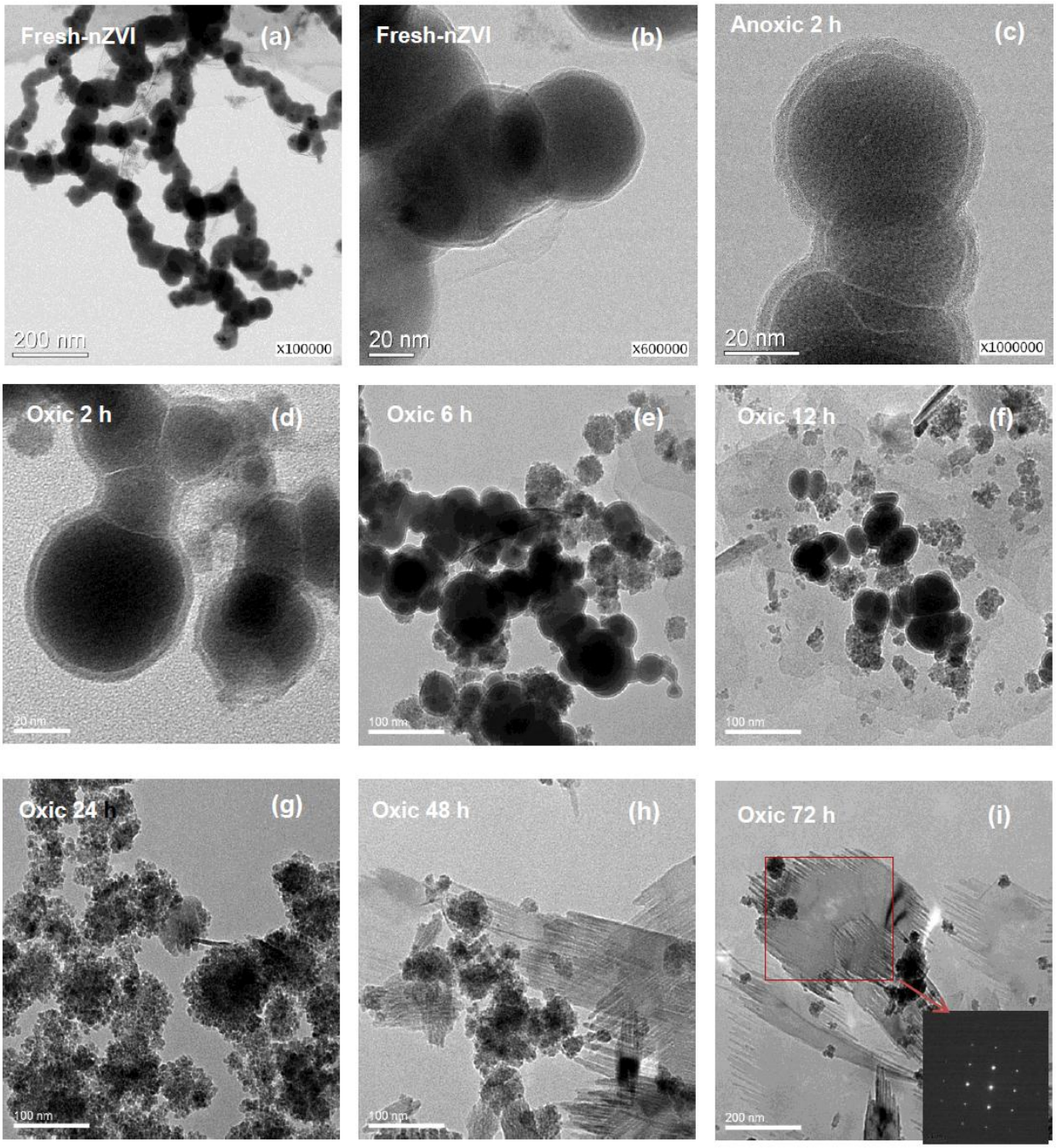

Fig. 1. TEM images of (a, b) fresh- nZVI, (c) nZVI eroded in anoxic water for 72 h, and (d-i) nZVI oxidized in oxic water over different time periods.

3.2 XRD analysis

Fig. 2 shows the XRD data of corrosion products of nZVI under oxic and anoxic water over a period of 72 h. Fig.2a contains the XRD patterns of fresh- and oxidized nZVI in oxic water. The broad peak of fresh nZVI at 2θ of 44°–45° proves the small particle size and size distributions of α-Fe^0 with indexes of (110) (JCPDS No. 06-0696) [6]. Meanwhile, the aged nZVI particles possess clear iron oxide/hydroxide peaks in the XRD patterns, which become more distinct and stronger with the progress of aging time. When put into water, some metal iron nanoparticles are oxidized into iron oxide/hydroxides. In the aqueous solution, Fe^{2+} is first formed on the surface, which reacts with H_2O/O_2 to form hydroxide or oxyhydoxide [28,29]. Representative reaction mechanisms may include:

$$Fe^0+2H_2O\rightarrow Fe^{2+}+H_2+2OH^- \quad (1)$$

$$Fe^0+O_2+2H_2O\rightarrow 2Fe^{2+}+4OH^- \quad (2)$$

$$6Fe^{2+}+O_2+6H_2O\rightarrow 2Fe_3O_4(s)+12H^+ \quad (3)$$

$$Fe^{2+}+2OH^-\rightarrow Fe(OH)_2(s) \quad (4)$$

$$6Fe(OH)_2(S)+2O_2\rightarrow 2Fe_3O_4+6H_2O \quad (5)$$

As seen in the XRD patterns, the intensity of the Fe^0 peaks gradually subsides. When the aging time is up to 24 h, the Fe^0 peaks start to disappear and peaks of magnetite (Fe_3O_4), maghemite (γ-Fe_2O_3) and lepidocrocite (γ-FeOOH) start to emerge (Fig. 2a).

It should be noted that the XRD patterns of Fe_3O_4 and γ-Fe_2O_3 in the nanoparticles cannot be clearly distinguished. It was reported that Fe_3O_4 can transform to γ-Fe_2O_3 [30]. Fe_3O_4 exists in an inverse spinel structure where the

Fe^{2+} is in an octahedral oxygen environment along with half of the Fe^{3+}. The other half of the Fe^{3+} exists in a tetrahedral oxygen environment. Oxidation of Fe^{2+} to Fe^{3+}, without a change in crystal structure, leads to γ-Fe_2O_3 [30]. In the presence of oxygen or other aqueous oxidants (Cr(VI), Ag(I), carbon tetrachloride), Fe_3O_4 magnetite may undergo topotactic oxidation to produce maghemite, as illustrated by the following reaction:

$$3Fe_3O_4+\frac{1}{2}O_2+2H^+\rightarrow 4\gamma\text{-}Fe_2O_3+Fe^{2+}+H_2O \quad (6)$$

Fe_3O_4 / γ-Fe_2O_3 and γ-FeOOH are detected in the particles aged for 48 to 72 h in the oxic water. However, the relative intensity of various mineral phases is different. γ-FeOOH is the predominant mineral until 48 h. The presence of γ-FeOOH as an oxidized product has been favored by the continuous supply of dissolved oxygen [Eqn. (7–9)] [31]:

$$4Fe^0+3O_2+2H_2O\rightarrow 4\gamma\text{-}FeOOH \quad (7)$$

$$4Fe_3O_4+O_2+6H_2O\rightarrow 12\gamma\text{-}FeOOH \quad (8)$$

$$\gamma\text{-}Fe_2O_3+H_2O\rightarrow 2\gamma\text{-}FeOOH \quad (9)$$

These results suggest that the corrosion of nZVI in oxygenated water clearly favors the formation of iron oxyhydroxide (FeOOH) over iron oxides. For nZVI aged over long periods of time, the eventual product in oxic water is mostly γ-FeOOH [27].

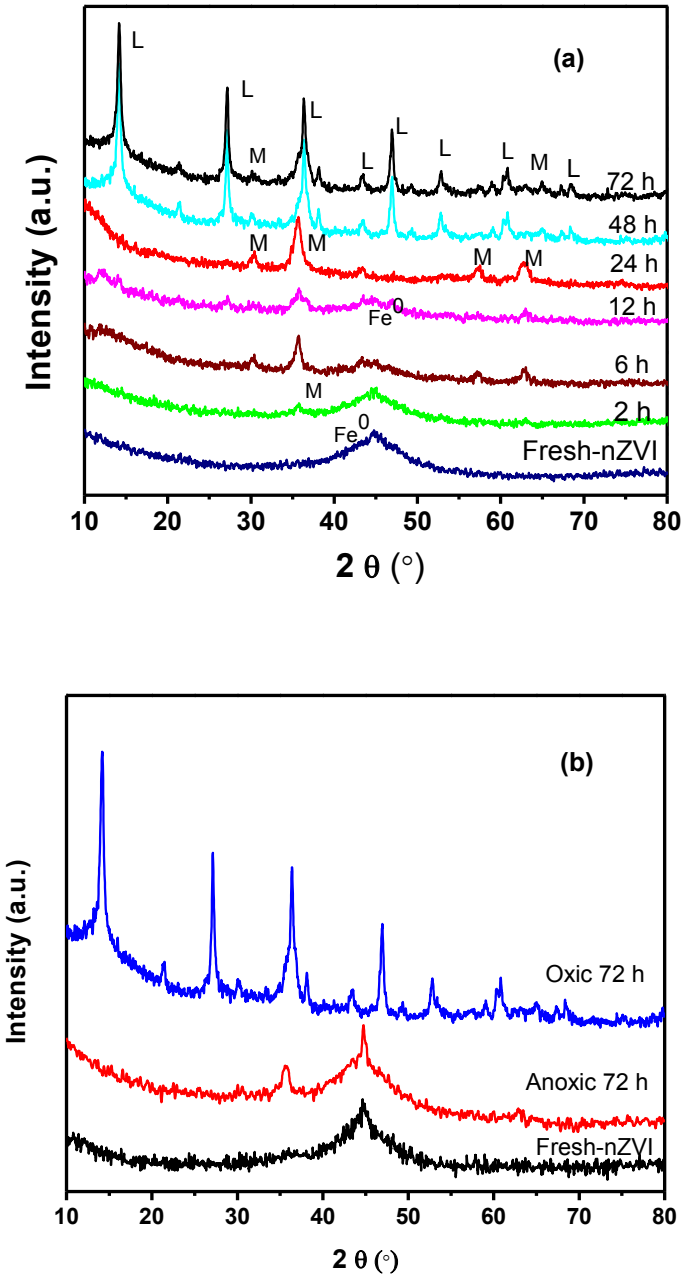

Fig. 2. (a) XRD analysis of fresh nZVI and oxidized nZVI as function of time in oxic water. Peaks are referred to magnetite/maghemite (Fe_3O_4/γ-Fe_2O_3) (M), lepidocrocite (γ-FeOOH) (L), and nZVI (Fe^0). (b) XRD analysis of fresh-nZVI, and nZVI under both anoxic and oxic water for 72 h.

Fig. 2b shows the XRD patterns of fresh- and 72-h-aged nZVI under anoxic and oxic conditions. In contrast to the sharp peaks of 72-h-aged nZVI under oxic condition, there is little difference between the 72-h-aged nZVI in anoxic water and fresh-nZVI. Results prove that the reaction rate between nZVI and water under the anoxic condition is slow. Relative small peaks of Fe_3O_4 are observed in Fig. 2b, which is consistent with previous report on the corrosion products in the anoxic environment [31]. However, the corrosion products vary and depend on the conditions under which the iron oxides were formed. The following Raman data can provide evidence on the formation of new products under anoxic conditions

3.3 Raman analysis

Raman spectroscopy is especially useful for characterizing poorly defined minerals or minerals not easily distinguished by conventional methods (e.g., XRD). The method has been widely used for the analysis of iron oxidation and scaling in steel corrosion processes [32].

The Raman spectra of fresh and corrosion products aged in oxic water are shown in Fig. 3a. Four clear bands at 217, 280, 388 and 595 cm^{-1} are observed in the Raman spectrum of nZVI particles aged less than 12 h. The combination of bands, at 220, 290, 300, and 412 cm^{-1} is best used for the identification of hematite. In this study the iron oxides, magnetite/maghemite (Fe_3O_4/γ-Fe_2O_3) are the mainly components within the shell of nZVI by the XRD data. The hematite detected by Raman spectra are ascribed to the transformation of the iron (oxy) hydroxides irradiated by laser, which demonstrates the absence of hematite in the XRD spectra. The band at 595

cm^{-1} appears in Raman spectra of nZVI aged for 12 h, which is the characteristic Raman peak of wustite. The peak of wustite is not found in XRD because the sensitivity of the XRD instrument may have been insufficient to detect small amounts of wustite [33]. Moreover, wustite is unstable. The presence of Fe(II) oxide provides the evidence that Fe(II) formation is an intermediate step in the nZVI evolution.

When the aging time increases up to 24 h, the new broad band from 660 to 710 cm^{-1} indicates co- existence of maghemite (γ-Fe_2O_3, 665, 730 cm^{-1}), magnetite (Fe_3O_4 ,670 cm^{-1}). The results are consistent with XRD results, which also demonstrate that Fe_3O_4 and γ-Fe_2O_3 are the major components for iron oxide shell in 1- to 24-h-aged products. When the nZVI aging time is prolonged to 48 h, or even up to 72 h, the peak positions at 250, 377, 526, and 650 cm^{-1} are in good agreement with the Raman spectra of lepidocrocite [34]. The typical Raman bands of the different iron oxide and (oxy)hydroxide phases are listed in Table 1.

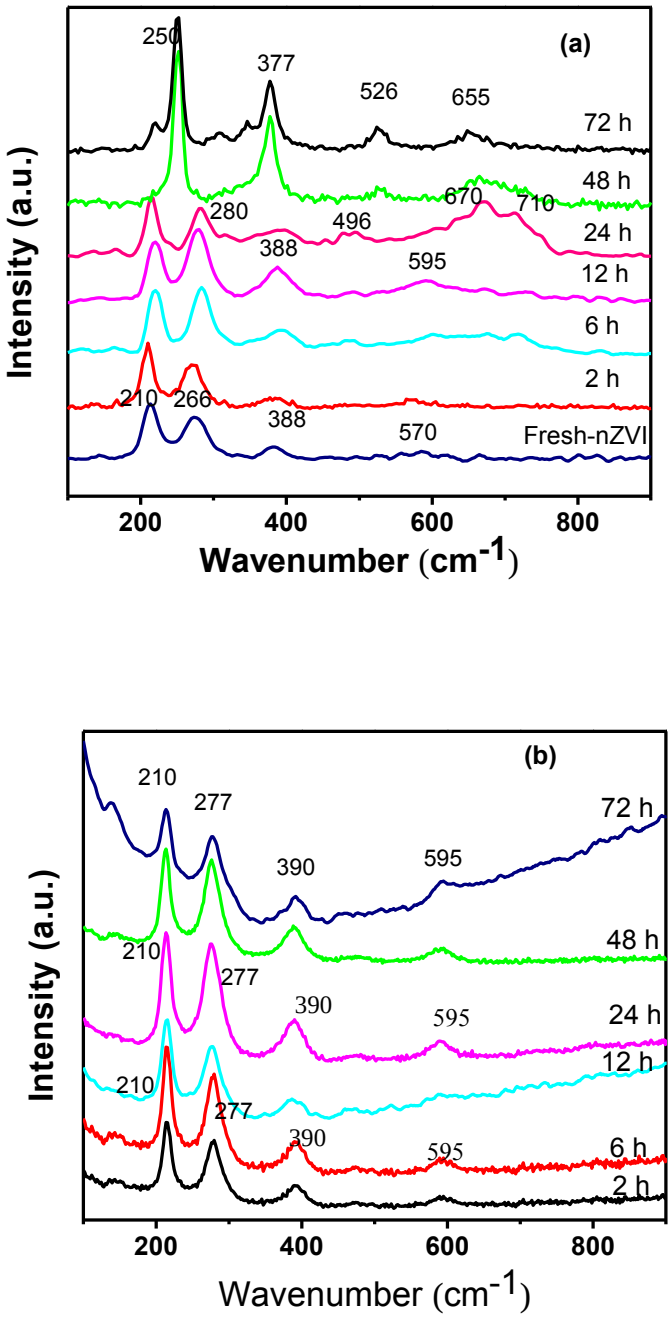

Fig. 3. Raman spectra of nZVI as a function of time under (a) oxic and (b) anoxic conditions ([nZVI]=5 g.L^{-1})

Fig. 3b shows the Raman spectra of nZVI aging in anoxic water from 2 to 72 h. Four bands are observed at 210, 280, 388 and 595 cm^{-1}. The clear band at about 390 cm^{-1} provides evidence on the existence of goethite/akaganeite in corrosion products. The peak at 595 cm^{-1}, which is the characteristic of FeO, is apparent under the anoxic condition while the anoxic condition favors the formation of FeO, *α*-FeOOH and *β*-FeOOH.

Table 1. Raman shifts for iron oxides and (oxy) hydroxides

Iron oxides & (oxy)hydroxides	**Raman shift (cm^{-1})**
Hematite (*α*-Fe_2O_3)	**210,** 276, 382, 1300
Lepidocrocite (γ-FeOOH)	**250,** 379, 526, 650
Goethite (*α*-FeOOH)	244 299 **385** 480 548 681
Akaganeite (*β*-FeOOH)	311,**390**,415,537, 614,717
Wuestite (FeO)	**595**
Magnetite (Fe_3O_4)	310 540 **670**
Maghematite (γ-Fe_2O_3)	350,512, **670** 720

Underlined and bold figures represent very strong while underlined figures represent strong. These results are typical for iron oxide [33, 34].

3.4 E_h and pH of the solution

Zero-valent iron (ZVI) is a reactive metal with a standard electrode potential, E_h^0, of -0.44V. Standard potential (often measured as ORP) has been widely used to assess the performance of nZVI [35]. The value of the ORP is sensitive to a number of fundamentally significant processes. Positive

values of ORP generally imply oxidizing conditions while negative ORP usually indicates reducing conditions in water. Under anoxic conditions typical of the subsurface environment, Fe(0) in nZVI quickly eliminates residual dissolved oxygen and reacts slowly with water. The zero-valent iron-mediated redox reactions produce a characteristic increase in solution pH and a concomitant decline in solution potential (E_h) [25].

In our experiments, a combination Ag/AgCl reference electrode is used in the monitoring of redox potential, and then the standard E_h is obtained by adding +202 mV to the measured redox potential readings [25]. According to Fig. 4a, the E_h value of the solution declines quickly (presumably due to a combination of rapid electrode polarization and solution equilibration effects) [35] after nZVI is placed into water, then approaches to a minimum value ($E_{h,min}$), usually within 20 min and remains stable after that. The $E_{h,min}$ values change with the aging time. When oxidized nZVI (less than 6 h) is put into water, $E_{h,min}$ of the solution is mostly in the range of -400 to -500 mV, close to that of fresh-nZVI. However, the addition of nZVI nanoparticles aged more than 24 h into water, produces $E_{h,min}$ only slightly lower than the initial value (50-200 mV). Results indicate that the nZVI nanoparticles are extensively oxidized to iron oxides after more than 24 h contacting with oxic water, which are consistent with the TEM pictures as well as XRD data. In oxic water after 24 h, nZVI is first transformed to the iron oxide spheres, then to flakey-shaped oxyhydroxides. The slight decrease of $E_{h,min}$ for nZVI aging from 24 to 72 maybe ascribe to the formation of different mineral phases of iron oxides in the oxic water.

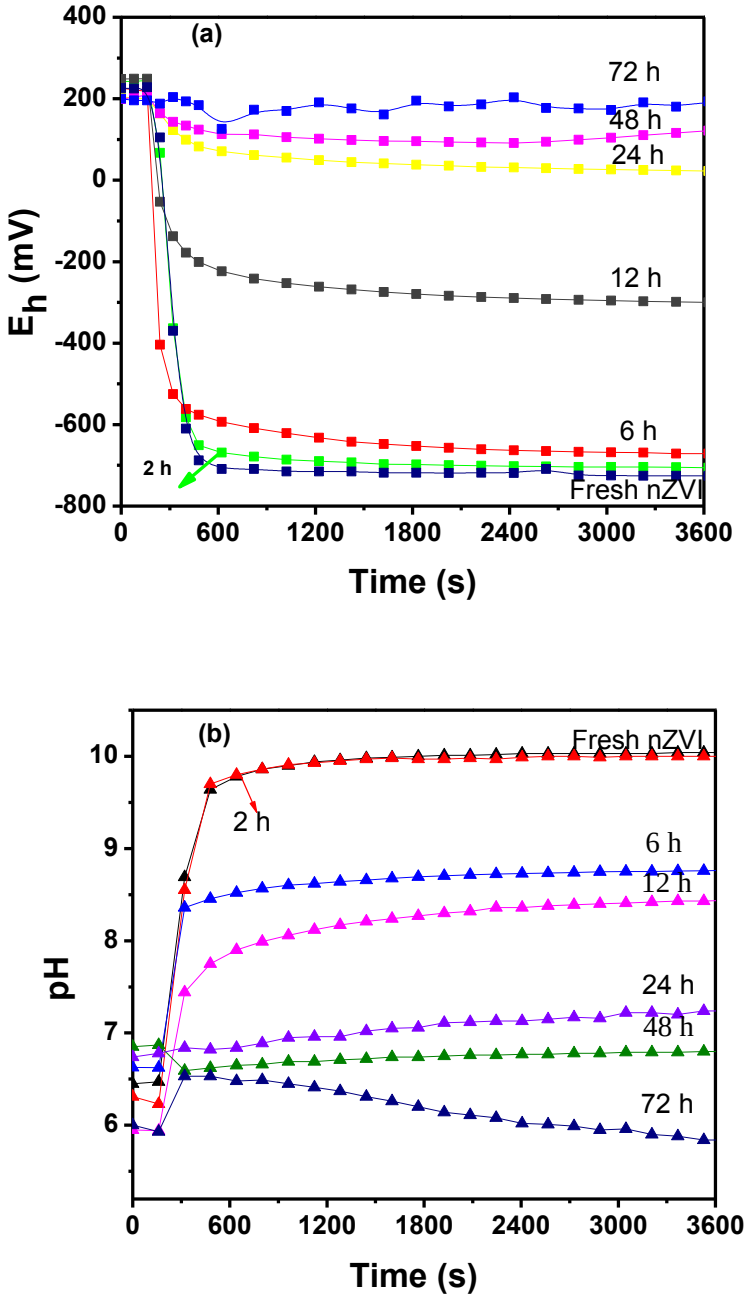

Fig. 4. E_h and pH of fresh- and nZVI particles under oxic water as function of time.

Our experiments show a typical increase in pH from ~6 to the range of 8–10 when nZVI (aging time <12 h) is put into solution. The addition of iron nanoparticles can generate hydrogen gas, produce divalent iron and lead to ascending solution pH. For the 24-h-aging nZVI, pH value of the solution is relatively stable at pH 7. Results show that the metallic iron in nZVI is fully consumed at this stage. The minor changes of solution pH for nZVI after 48 and 72 h aging maybe ascribe to the dissolution of iron oxides.

3.5 Reaction mechanisms

A conceptual model on the transformation of nZVI in water is illustrated in Fig. 5, which highlights the experimental results obtained in the study. The formed mineral phases on the particle surface and the core-shell structure of nZVI vary with the aging progress and environmental conditions. Fresh nZVI has a core-shell structure with spherical shape. The core-shell structure can be maintained over an extended period of time (e.g., 72 h) under anoxic condition. The oxidation products of nZVI in anoxic water for 72 h are the mixture of FeO, α-FeOOH and/or β-FeOOH. Under oxic conditions, the core-shell structure transforms into the circular spheres composed of magenetite/maghemite when aging time is up to 24 h. After 48 h aging in water, the spheres of iron oxides evolve into new flaky and/or acicular-shaped phases. With continuously supply of oxygen for nZVI in water, the products are mainly of flaky-shaped lepidocrocite, γ-FeOOH.

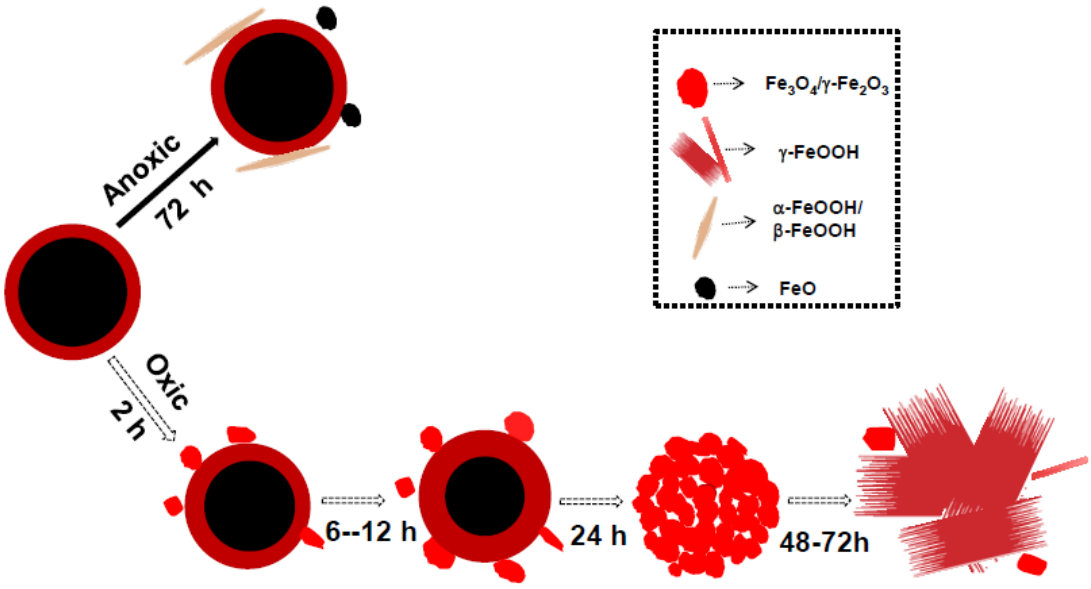

Fig.5. A conceptual model on nZVI evolution in water

4. Conclusions

Evolution of nZVI in water is studied by TEM, XRD, and Raman spectroscopy. Reactions at the nZVI/water interface influence the core-shell structure and the corrosion products. Images acquired by TEM provide detailed morphological and structural changes with the progress of time. Under anoxic conditions, the core-shell structure of nZVI is well maintained after 72 h. Under oxic conditions, the core-shell structure quickly evolves. The particles may maintain the spherical shape at the initial corrosion stage, and eventually evolve into flaky and/or acicular-shaped structures. XRD and Raman spectra provide evidence that the components of corrosive nZVI vary with the aging time. The corrosion products of nZVI in anoxic water for 72 h are a complex mixture of FeO, α-FeOOH or/and β-FeOOH. Under oxic conditions, γ-FeOOH is the primary final product. The patterns of SAED prove the single crystal of the product for 72 h oxidizing in water. Information on the componential, morphological, and structural evolution of nZVI under different conditions

generates a detailed physical model of nZVI under different environments.

Acknowledgements

Research described in this work has been partially supported by the National Science Foundation of China (NSFC Grants 21277102, 21003151), the Science and Technology Commission of Shanghai (Grant 11JC1412600), and the Collaborative Innovation Center for Regional Environmental Quality.

References

1. W.L. Yan, H.-L. Lien, B.E. Koel, W.-X. Zhang, Iron nanoparticles for environmental clean-up: recent developments and future outlook, Environ. Sci.: Processes Impacts, 15 (2013) 63–77.
2. M. Khin, A.S. Nair, V.J. Babu, R. Murugan, S. Ramakrishna, A review on nanomaterials for environmental remediation, Energy & Environ. Sci., 5 (2012) 8075–8109.
3. L. Ling, W.-X. Zhang, Enrichment and Encapsulation of Uranium with Iron Nanoparticle, J. Am. Chem. Soc., 137 (2015) 2788-2791.
4. W.-X. Zhang, Nanoscale iron particles for environmental remediation: an overview, J. Nanopart. Res., 5 (2003) 323-332.
5. A.R. Liu, W.-X. Zhang, Fine structural features of nanoscale zero-valent iron characterized by spherical aberration corrected scanning transmission electron microscopy (Cs-STEM), Analyst, 139 (2014) 4512-4518.
6. X.Q. Li , W.-X. Zhang, Iron nanoparticles: the core-shell structure and unique properties for Ni (II) sequestration, Langmuir, 22 (2006) 4638-4642.
7. B.C. Reinsch, B. Forsberg, R.L. Penn, C.S. Kim, G.V. Lowry, Chemical transformations during aging of zerovalent iron nanoparticles in the

presence of common groundwater dissolved constituents Environ. Sci. Technol., 44 (2010) 3455–3461.

8. N. Kumar, M. Auffan, J. Gattacceca, J. Rose, L. Olivi, D. Borschneck, P. Kvapil, M. Jublot, D. Kaifas, L. Malleret, P. Doumenq, J.-Y. Bottero, Molecular Insights of Oxidation Process of Iron Nanoparticles: Spectroscopic, Magnetic, and Microscopic Evidence, Environ. Sci. Technol., 48 (2014) 13888-13894.
9. V. Sarathy, P.G. Tratnyek, J.T. Nurmi, D.R. Baer, J.E. Amonette, C.L. Chun, R.L. Penn, E.J. Reardon, Aging of iron nanoparticles in aqueous solution: effects on structure and reactivity, J. Phys. Chem. C, 112 (2008) 2286–2293.
10. L.F. Greenlee, J.D. Torrey, R.L. Amaro, J.M. Shaw, Kinetics of zero valent iron nanoparticle oxidation in oxygenated water, Environ. Sci. Technol., 46 (2012) 12913−12920.
11. J. Klausen, P.J. Vikesland, T. Kohn, D.R. Burris, W.P. Ball, A.L. Roberts, Longevity of granular iron in groundwater treatment processes: solution composition effects on reduction of organohalides and nitroaromatic compounds, Environ. Sci. Technol., 37 (2003) 1208-1218.
12. T. Kohn, K.J.T. Livi, A.L. Roberts, P.J. Vikesland, Longevity of granular iron in groundwater treatment processes: corrosion product development, Environ. Sci. Technol., 39 (2005) 2867-2879.
13. Q.L. Wang, S. Snyder, J. Kim, H. Choi, Aqueous ethanol modified nanoscale zerovalent iron in bromate reduction: synthesis, characterization, and reactivity, Environ. Sci. Technol., 43 (2009) 3292–3299.

14. K.H. Sohn, S.W. Kang, S.Y. Ahn, M.W. Woo, S.K. Yang, Fe(0) nanopartcles for nitrate reduction: Stability, reactivity, and transformation, Environ. Sci. Technol., 40 (2006) 5514–5519.
15. H.-S. Kim, J.-Y. Ahn, K.-Y. Hwang, I.-K. Kim, I. Hwang, Atmospherically stable nanoscale zero-valent iron particles formed under controlled air contact: characteristics and reactivity Environ. Sci. Technol., 44 (2010) 1760–1766.
16. Y. Xie, Z. Fang, X. Qiu, E.P. Tsang, B. Liang, Comparisons of the reactivity, reusability and stability of four different zero-valent iron-based nanoparticles, Chemosphere, 108 (2014) 433-436.
17. l. Zhou, T.L. Thanh, J. Gong, J.H. Kim, E.J. Kim, Y.S. Chang, Carboxymethyl cellulose coating decreases toxicity and oxidizing capacity of nanoscale zerovalent iron, Chemosphere, 104 (2014) 155–161.
18. H.-S. Kim, J.-Y. Ahn, K.-Y. Hwang, I.-K. Kim, I. Hwang, Aging characteristics and reactivity of two types of nanoscale zero-valent iron particles (Fe^{BH} and Fe^{H2}) in nitrate reduction, Chem. Eng. J., 197 (2012) 16–23.
19. Q.L. Wang, S. Lee, H. Choi, Aging Study on the Structure of Fe^{0}-Nanoparticles: Stabilization, Characterization, and Reactivity, J. Phys. Chem. C, 114 (2010) 2027-2033.
20. B.C. Reinsch, B. Forsberg, R.L. Penn, C.S. Kim, G.V. Lowry, Chemical Transformations during Aging of Zerovalent Iron Nanoparticles in the Presence of Common Groundwater Dissolved Constituents, Environ. Sci. Technol., 44 (2010) 3455–3461.

21. A.R. Liu, J. Liu, W.-X. Zhang, Transformation and composition evolution of nanoscale zero valent iron (nZVI) synthesized by borohydride reduction in static water, Chemosphere, 119 (2015) 1068-1074.
22. L.F. Greenlee, J.D. Torrey, R.L. Amaro, J.M. Shaw, Kinetics of Zero Valent Iron Nanoparticle Oxidation in Oxygenated Water, Environ. Sci. Technol., 46 (2012)12913–12920.
23. S.L. Li, W. Wang, Y.Y. Liu, W.-X. Zhang, Nanoscale zero-valent iron (nZVI) for the treatment of concentrated Cu(II) wastewater: a field demonstration, Environ. Sci.: Processes Impacts, 16 (2014) 524-533.
24. S.L. Li, W. Wang, Y.Y. Liu, W.L. Yan, Zero-valent iron nanoparticles (nZVI) for the treatment of smelting wastewater: A pilot-scale demonstration, Chem. Eng. J. 254 (2014) 115-123.
25. Y.P. Sun, X.Q. Li, J.S. Cao, W.-X. Zhang, H.P. Wang, Characterization of zero-valent iron nanoparticles, Adv. Colloid Interfac., 120 (2006) 47-56.
26. D.D. Boland, R.N. Collins, C.J. Miller, C.J. Glover, T.D. Waite, Effect of solution and solid-phase conditions on the Fe(II)-accelerated transformation of ferrihydrite to lepidocrocite and goethite, Environ. Sci. Technol., 48 (2014) 5477–5485.
27. A.R. Liu, J. Liu, B.C. Pan, W.-X. Zhang, Formation of Lepidococite (γ-FeOOH) from Oxidation of Nanoscale Zero-Valent Iron (nZVI) in the Oxygenated Water, RSC Adv., 4 (2014) 57377-57382.
28. S.R. Kanel, B. Manning, L. Charlet, H. Choi, Removal of arsenic(III) from groundwater by nanoscale zero-valent iron, Environ. Sci. Technol., 39 (2005) 1291-1298.
29. B.A. Manning, M.L. Hunt, C. Amrhein, J.A. Yarmoff, Arsenic(III) and

arsenic(V) reactions with zerovalent iron corrosion products, Environ. Sci. Technol., 36 (2002) 5455-5461.

30. D.Q. Yang, E. Sacher, Uniformly Dispersed Pt−Ni Nanoparticles on Nitrogen-Doped Carbon Nanotubes for Hydrogen Sensing, J. Phys. Chem. C, 114 (2009) 6418-6425.
31. Y.H. Huang, T.C. Zhang, Effects of dissolved oxygen on formation of corrosion products and concomitant oxygen and nitrate reduction in zero-valent iron system, Water Res., 39 (2005) 1751-1760.
32. M.K. Nieuwoud, J.D. Comins, I. Cukrowsk, The growth of the passive film on iron in 0.05 M NaOH studied in situ by Raman micro-spectroscopy and electrochemical polarisation. Part I: near-resonance enhancement of the Raman spectra of iron oxide and oxyhydroxide compounds, J. Raman Spectrosc., 42 (2011) 1335-1339.
33. H. Monika, Raman spectroscopy of iron oxides and (oxy) hydroxides at low laser power and possible applications in environmental magnetic studies, Geophys. J. Int., 77 (2009) 941-948.
34. Y.S. Li, J.S. Church, A.L. Woodhead, Infrared and Raman spectroscopic studies on iron oxide magnetic nano-particles and their surface modifications, J. Magn. Magn. Mater., 324 (2012) 1543-1550.
35. Z. Shi, J.T. Nurmi, P.G. Tratnyek, Effects of nano zero-valent iron on oxidation−reduction potential, Environ. Sci. Technol., 45 (2011) 1586-1592.

Graphical Abstract